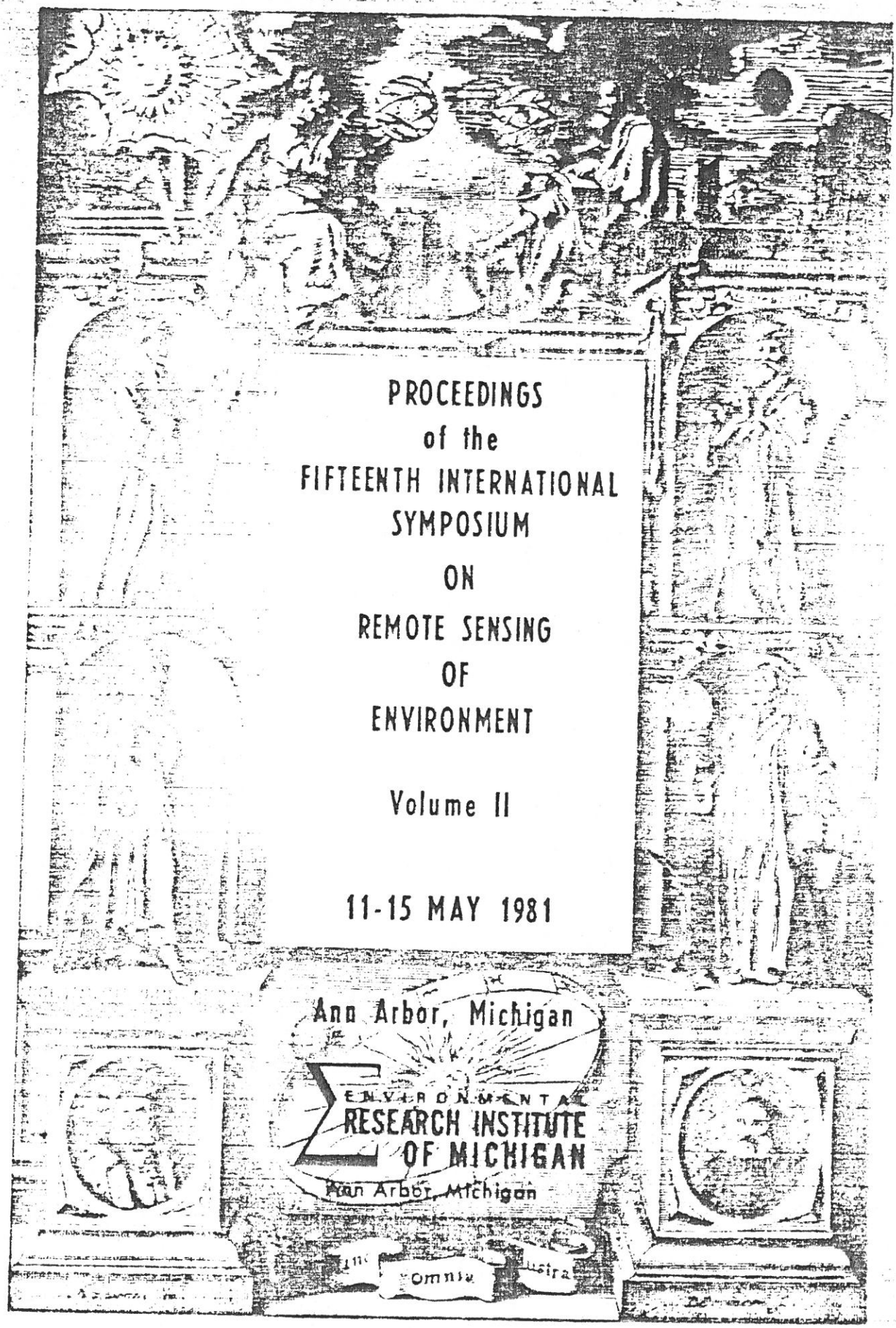
PROCEEDINGS
of the
FIFTEENTH INTERNATIONAL
SYMPOSIUM
ON
REMOTE SENSING
OF
ENVIRONMENT
Volume II
11-15 MAY 1981
Ann Arbor, Michigan
ENVIRONMENTAL
RESEARCH INSTITUTE
OF MICHIGAN
Ann Arbor, Michigan

GROUND-BASED LIDAR FOR UPPER ATMOSPHERIC DENSITIES*

G. W. Bethke, R. L. Franklin, and L. W. Springer
General Electric Company
Space Systems Division
King of Prussia, PA, USA

C. R. Philbrick and J. P. McIsaac
Air Force Geophysics Laboratory
Hanscom AFB, MA, USA

ABSTRACT

A ground-based lidar system has been designed which will be capable of determining upper atmosphere densities from 20 km to about 100 km altitude even in the presence of high altitude haze, and will do so with only 15 minutes total measurement time. Furthermore, this system will contain real time automatic data processing, capability for near-real time data reduction, and will be compact enough to be compatible with eventual modification for mobility. Thus this lidar system will provide a unique combination of measurement range, tolerance for haze interference, moderate physical size, measurement speed, and special data handling and reduction electronics for upper atmosphere density measurements.

1. INTRODUCTION

For several years, ground-based lidar systems have been used to obtain upper atmospheric density profiles[1-3] to altitudes as great as 100 km.[4] Such long range measurements are generally based on Rayleigh backscatter from upper atmospheric air molecules and must often require the assumption of no significant upper atmospheric haze. For the highest altitude capabilities, such lidar systems tend to be very large and/or require long measurement times.

To facilitate the study of upper atmosphere dynamics, a ground-based lidar system has been designed for relatively rapid measurements, even in the presence of high altitude haze. Some desired characteristics for such a lidar system include the following:

- measure high altitude atmospheric density,
- measurement altitude range = 20-100 km,
- altitude resolution = 0.5 km at 20 km to 2.5 km at 100 km,
- measurement time = 5 minutes at 20 km to 15 minutes (max) at 100 km,
- measure all altitude ranges simultaneously,
- maximum random error = 4% at 20 km to 10% at 100 km,
- minimize costs.

Briefly, the design features which allow the above needs to be met with a reasonably compact and relatively inexpensive lidar include:

- use of the two-color lidar concept (355 nm and 532 nm),
- both wavelengths are from the same laser,

*Presented at the Fifteenth International Symposium on Remote Sensing of Environment, Ann Arbor, MI, May, 1981.

- use of high efficiency optics throughout to reduce required telescope size (cost),
- detection employs photon counting,
- use of digital data processing,
- stationary lidar site (cost),
- fixed vertical pointing direction only (cost).

An additional feature is that the system will provide on-site data reduction.

2. SPECIAL CONSIDERATIONS

2.1 LIDAR THEORY

The "range" equation which relates lidar receiver output N_s to lidar and atmospheric properties is

$$N_s = [\pi/(8h)](d/r)^2 \, k_b \, \lambda_s \, U \, E_o T_i T_s \qquad (1)$$

where

$$r = c\,t/2. \qquad (2)$$

For Rayleigh plus Mie (haze) scatter ($\lambda_i = \lambda_s$),

$$k_b = n\,Q_{rb} + m\,Q_{mb} = K_r\, n\, \lambda^{-4} + K_m\, m\, \lambda^{-a} \qquad (a \lesssim 1) \qquad (3)$$

Here, N_s is lidar receiver detected count rate in photons/second, h is the Planck constant, d is diameter of lidar receiver aperture, r is measurement range, k_b is atmospheric backscatter coefficient, λ_i and λ_s are incident and scattered light wavelengths respectively, U is laser output energy per pulse, E_o is lidar system efficiency including the detector quantum efficiency (QE), T_i and T_s are one-way atmospheric transmittance from the lidar to range r at λ_i and λ_s respectively, c is the velocity of light, t is time, n and m are atmospheric and aerosol total densities respectively, Q_{rb} and Q_{mb} are Rayleigh and Mie (aerosol) backscatter cross sections respectively, and the various K's are constants.

Combining equations (1) and (3), we see that for photon-counting lidar systems, the lidar signal component due to atmospheric gas varies as $1/\lambda^3$, while the component due to aerosol is approximately independent of wavelength. This difference in wavelength dependence together with the use of two lidar wavelengths makes possible the extraction of the Rayleigh(gas)-scattered component from lidar signals containing moderate levels of haze (aerosol scatter). The resulting correction for haze has limited accuracy because the exact value of the haze wavelength parameter a (Eq. 3) varies with aerosol particle shape, size distribution, composition, and wavelength. Fortunately above about 5 km altitude, and especially above 30 km, the clear air aerosol levels are such that in the UV, blue and green, ususally $(m\,Q_{mb}) < (n\,Q_{rb})$. Thus if the lidar is calibrated at the high altitudes of use and the subsequent changes in T are monitored, then the relatively small haze corrections are within the capabilities of a UV-visible two-wavelength Rayleigh-scatter lidar system. In this manner, full advantage can be taken of the long range high performance capabilities of a Rayleigh-based density-measuring lidar system.

By again combining equations (1) and (3) and noting that $E_o = E_f \cdot (QE) \cdot E(\text{optics})$, the gas density-sensitive Rayleigh-scattered component N_{sr} of the lidar signal is seen to be a function of only a few λ-sensitive parameters.

$$N_{sr} = K[\lambda^{-3} T^2 E_f \cdot (QE)]U = K\, E_m\, U \qquad (4)$$

Here, $T = T_i = T_s$, E_f is bandpass filter optical efficiency, (QE) is detector quantum efficiency, and K is a constant largely independent of λ. Thus $E_m \cdot U$ is a relative measure of lidar efficiency for obtaining N_{sr}.

Figure 1 shows a plot of E_m vs wavelength (solid line) throughout the visible and near-visible, as well as of the various components (dashed lines) of E_m. Here, T is vertical atmospheric transmittance from sea level to space, E_f is typical for good bandpass filters, and (QE) values are the best commercially available in photomultiplier tubes. In addition, the laser times efficiency product ($U \cdot E_m$) values are plotted in Figure 1, where U values are maximum useful outputs per second (100 pps max.) from commercially available pulsed lasers (400 nsec max. pulse width). As seen in Figure 1, the best pair of $E_m \cdot U$ points from a single laser are from a pulsed Nd:YAG laser frequency doubled and tripled for outputs at 532 nm and 355 nm.

2.2 LIDAR SYSTEM NOISE

Lidar systems operating in the near infrared, visible, and ultraviolet spectral regions usually use photomultiplier tube detectors due to their relatively high quantum efficiencies and relatively noise-free high gain. As a result, high sensitivity photomultiplier tubes can detect individual photons when illuminated by low light levels. In this case, the primary noise is due to the statistical fluctuations in arrival of the individual photons (yielding shot noise). Thus assuming Poisson statistics, the standard deviation variation or noise count, N , in a specific time (lidar range) interval is

$$N = \sqrt{S} \tag{5}$$

where

$$S = N_s + N_b + N_d \tag{6}$$

Here, S is the average count from the sum of signal counts N_s, background counts N_b, and detector dark counts N_d.

The percent random error referred to earlier is $\pm 100/(S/N)$, where for signal counts only, the signal-to-noise ratio is

$$S/N = N_s/\sqrt{N_s} = \sqrt{N_s} \tag{7}$$

Including background and dark current effects,

$$S(N_s)/N = (S - N_b - N_d)/(S + N_b + N_d)^{\frac{1}{2}} \tag{8}$$

In the presence of such competing photon sources, the (S/N) ratio can be improved by averaging over several (n) background measurements for each signal measurement.

$$S(N_s)/N = [S - (N_b + N_d)]/[S + (N_b + N_d)/n]^{\frac{1}{2}} \tag{9}$$

The (S/N) improvement resulting from this technique becomes greater as the background becomes larger relative to the signal.

The lidar background photon count rate due to diffuse sky radiation is

$$N_b = [\pi^2/(16hc)]\, I_s\, \lambda\, B\, d^2\, \alpha^2\, E_r \tag{10}$$

where I_s is sky radiance at wavelength λ, B is the receiver spectral bandpass, α is the full angle field-of-view (fov) of the lidar receiver, and E_r is lidar receiver efficiency including the detector. If background is a problem such as during the daytime, this equation shows the benefit from minimizing the receiver fov and system bandpass.

3. SYSTEM DESIGN

3.1 OPTICAL DESIGN

Briefly, the lidar system is to use an up-collimated Neodymium:YAG frequency doubled and tripled laser beam as the two-wavelength light source, a

large aperture compound reflecting telescope as the lidar receiver, and an array of photomultiplier tube (PMT) detectors with beam splitters and narrow band filters for spectral isolation.

Table I. Lidar Characteristics

Laser		
Type laser	Neodymium:YAG (pulsed)	
Simult. outputs at 10 pps		
at 1064 nm	0.45 J/pulse	
at 532 nm	0.40 J/pulse	
at 355 nm	0.22 J/pulse	
Pulse lengths	all 15 nsec	
Beam diameter	9.5 mm (3/8 inch)	
Beam divergence	0.6 mrad full angle	
Output polarization	horizontal (355 & 532 nm)	
Energy monitor (WE) detectors	Si photodiodes (one each λ)	
Beam Expander		
Type	all-reflective off-axis	
Beam expansion	15 times	
Expanded beam divergence	0.04 mrad full angle	
Receiving Telescope		
Type	Dall Kirkham reflector	
Collecting aperture	91.4 cm (36") diam.	
Field-of-view	0.2 mrad full angle	
Field stop (FS)	0.3 cm diam. (approx.)	
Dichroic Mirror (DM)		
Reflectance	99% at 355 nm	
Transmittance	≥85% at 532 nm	
Interference Filters (Fig. 2)	FG	FU
Transm. peak wavelength	532 nm	355 nm
Bandpass width (FWHH)	2.5 nm	5.0 nm
Peak transmittance	≥60%	≥25%
Photomultiplier Tubes (PMTs)		
PMT models	RCA-8850	VPM-152S
Cathode type	bialkali	GaAsP
Cathode quantum eff.		
at 355 nm	32%	40%
at 532 nm	10%	35%
Dark count rates (cps)		
at 20° to 22°C	170(20)[a]	5000
at -20°C	N/A	10
PMT numbers (see Fig. 2)		
for 355 nm use	1, 2, & 3	none
for 532 nm use	4 & 5	6

Notes: (a) as reduced with use of magnetic defocusser.

As detailed in Table I, a two-color laser output is to be used, this being supplied by a commercially-available Nd:YAG laser which is capable of simultaneous large outputs at both 532 nm (green) and 355 nm (near UV) at a 10 pps repetition rate. Figure 2 illustrates how the laser output will pass through a laser energy monitor WE and then through an up-collimating beam expander to decrease laser beam divergence. After leaving the beam expander, the laser beam will reflect off adjustable flat mirror FM so as to become parallel to the adjacent receiver telescope axis. This adjustable mirror is the means by which the

lidar laser is boresighted to the lidar receiver. For eye safety, a small microwave radar transceiver is also recommended so as to provide automatic abort of laser system output when an aircraft nears the laser beam.

After the backscattered laser light plus any background light is reflected off the receiver primary mirror PM to the secondary mirror SM, the light is focused through the telescope indoor/outdoor window WT onto field stop FS. This focus is also near shutter wheel SW(A). After passing through FS, the now diverging light is collimated by lens CL and then directed to several detectors PMT-1 through PMT-6 via a dichroic mirror DM, flat mirror FM, bandpass filters FG and FU, a series of beam splitting mirrors BS, some intensity-adjusting neutral filters NF, detector lenses DL, and in some cases also through relay lenses RL. The purpose of the four beam splitters BS is to apportion the light between the three PMT's, which are provided for each wavelength, in such a manner that each PMT is used at an optimum light intensity during its assigned lidar altitude interval.

The RCA-8850 and Varian VPM-152S detectors to be used (see Table I) were primarily chosen for their combination of high quantum efficiency, low background, fast response, relatively good photo-electron collecting efficiency, and good first dynode gain. It should be noted that the typically quoted photo-cathode quantum efficiencies (QE) are often not achieved in practice due to imperfect electron-collection efficiency by the first dynode. The linear focused PMT's chosen here are both estimated to have first dynode collection efficiencies of about 0.9. The RCA-8850 PMT has such a high first dynode gain that it is estimated to have a counting efficiency of one, for an overall efficiency of 0.9 x (QE). Since the VPM-152S PMT has a less high first dynode gain, its counting efficiency is estimated as 0.9, for an overall efficiency of 0.81 x (QE) = 28.4% at 532 nm.

Again referring to Figure 2, a synchronized pair of 28 cm diam. rotating shutter wheels [SW(A) and SW(B)] will protect the light-sensitive PMT detectors from the relatively intense near-range lidar signals. The common shutter wheel shaft will be driven through a geared belt by an electric motor. Use of a constant voltage transformer plus variable autotransformer will allow stable but somewhat adjustable shutter speed. At a nominal 7000 rpm, shutter SW(A) will uncover the 3 mm field stop FS in 32 microseconds (4.8 km lidar range interval). Shutter SW(A) will be set to unblock FS by an altitude (Z) of 20 km, while SW(B) will unblock the two highest altitude-sensing PMT's by Z=50 km. An LED source plus double photodiode detector senses SW(A) position, and provides a timing pulse for the lidar system controller (see later).

Since the lidar receiving telescope will have an aluminum structure and be subject to outdoor temperatures, its focus will shift axially by about +0.11 cm/^{o}C. Thus the total variation in focus during the year can be quite large. When such an axial focus shift becomes too large relative to the detector section field stop FS, the focus shift will be accommodated by moving the entire detector section along guide rails which are parallel to the telescope axis.

3.2 ELECTRONICS AND DATA ACQUISITION

As indicated in Figure 3, the six photomultiplier (PMT) photon pulse outputs (see Figure 2) plus the green and UV laser energy (U) monitor outputs are fed through fast discriminator circuits into two multiplexers, one for the green signal detectors and the other for the UV signal detectors. As the scattered light signals weaken from both (green and UV) receding laser light pulses, each multiplexer switches at pre-determined intervals (t_0 plus about 220, 350, and 700 microseconds) from its least sensitive (low Z) PMT, to its mid-range PMT, to its highest sensitivity (high Z) PMT, and then finally to its laser energy monitor output. Switching will take less than 100 nsec. The output from each laser energy monitor is "digitized" by proportional conversion to a pulse frequency. This "digitizing" output is then held until after the multi-

plexer completes its energy sampling period.

The data acquisition and storage (DAS) system will incorporate two scalers, one for each laser wavelength, and each with 100 mHz count rate capability. Overall, the DAS system will have an 8000 channel storage capacity with a cumulative memory of 2^{24} counts per channel, a 2 microsecond minimum dwell time per channel (when two scalers used), and only 5 nsec dead time between channels. It will also have a CRT display capacity, floppy discs for data management and data reduction software as well as for long term storage of raw and/or reduced data, and a printer/plotter for paper records.

Normally, the lidar system will only use about 700 channels for signal data, 700 channels for background measurement data, and 1000 channels for laser energy data. The cumulative count levels will not exceed 900,000 = $<2^{20}$ per channel per lidar run.

The basic requirements of the lidar "system controller" (see Figure 3) are to synchronize the events in the lidar system with the shutter wheel, decide how shutter opportunities should be used (laser shot, background shot or nothing), count the number of events and compare it with a preset value, provide timing for the complete data acquisition system and supply the proper delays for different control signals. Each laser or background trigger from the system controller re-sets (enables) the scalers and multiplex (MPX) controller, as well as pre-sets the DAS unit for either lidar laser shot or background channels. The laser and background t_0 signals (see Figure 3) start the system clock which initiates and controls the MPX controller and the DAS system. When the preset number of laser shots has occurred, the system controller will then interrupt the laser beam and stop the data acquisition.

Between lidar runs, the DAS system can use its floppy disc software to perform data reduction.

3.3 INSTALLATION

To minimize costs and complexity, this lidar system is designed for fixed site use (initially at AFGL, Hanscom AFB), and will be of fixed vertical orientation for probing the atmosphere in the zenith direction. As indicated in Figure 2, the laser and beam expander will be oriented in the normal horizontal position, with the adjustable beam-deflecting flat mirror FM being used to boresight the expanded laser beam to the vertically-oriented receiving telescope.

Before and during lidar runs, the receiving telescope, the deflecting mirror FM, and the laser beam expander will all be exposed to outdoor ambient temperatures through a large coverable opening in the ceiling. However, to provide a better environment for all the other subsystems and equipment as well as for the operators, the laser, the receiver detection section, and all electronics will be located in air conditioned areas behind insulated walls and partitions. Referring to Figure 2, the window WE which forms part of the laser output energy monitor will be located in such an insulated panel, as will be the telescope near-focus window WT. The use of a controlled environment will sufficiently stabilize the bandpass filters and most detectors without the need for special housings, will prevent cooling water from freezing during storage periods, will provide the stable room temperature operating environment required by the laboratory-quality laser, and will easily meet the environmental requirements of all electronics, including the DAS system's relatively sensitive floppy disc memory unit.

This entire lidar system will weigh about 1800 kg, will occupy less than 30 square meters floor space, and could be re-configured for mobility in a large trailer.

3.4 CALIBRATION

The lidar system plus lower atmosphere (below 20 km) are to be jointly calibrated by making normal lidar measurements of 20 km altitudes and above, while "ground" truth reference measurements of atmospheric density are made at two differing altitudes above 20 km. These ground truth measurements can be obtained with either rocket or balloon-borne instruments, as long as both measurements are obtained close enough in time and space to the lidar measurement to be applicable.

Ground truth reference measurements are needed at two altitudes because the probable presence of significant haze backscatter during calibration requires combining the two range equations (one for each lidar wavelength) to eliminate the unknown haze scatter coefficients. Now with one combined equation containing two calibration constants (one for each wavelength), reference data are needed from two altitudes to permit a solution. The two reference altitudes should have significantly different atmospheric density, but negligible attenuation between them.

Since the combined lidar plus lower atmosphere (<20 km) calibration is valid only as long as the lower atmosphere vertically integrated absorption is constant, the calibration may have to be repeated each night. However, if the lower atmosphere integrated transmittance is monitored at the lidar wavelengths, then the lidar calibration constants could be corrected for changes in atmospheric transmittance, and the calibration remain valid for extended periods of time.

A simple method for monitoring the atmospheric total transmittance is by measurement of star intensities using a special small pointable telescope complete with detector and lidar wavelength filters. If the intensities of several stable stars are measured during a lidar calibration run, then later reference to any of those stars will permit correction of the lidar calibration constants for changes in atmospheric transmission. It is here assumed that while star intensity is affected by the total atmosphere (from ground level on up), essentially all the attenuation changes are due to the lowest 20 km. Also, as star elevation changes during the night and/or season, correction must be made for non-vertical slant path effects on transmittance.

4. ANTICIPATED PERFORMANCE

The anticipated lidar performance has been calculated using the equations presented earlier. These results are shown in Figure 4 as percent random error vs altitude of the backscattered signal (N_S) in the presence of anticipated detector dark counts (see Table I) and various types of sky background. Two of the photomultiplier tube (PMT) switching altitudes (Z_S) are indicated in Figure 4 by A and B.

From equation (9), we define the percent random error (%RE) as

$$(\%RE) = 100/[S(N_s)/N]$$

$$= 100[N_s + (N_b + N_d)(n+1)/n]^{\frac{1}{2}}/N_s \qquad (11)$$

where we here use n=10 background plus dark count samples per laser shot. For these calculations, the laser repetition rate is 10 pps, N_S for each shot is calculated using Eq. (1) and the LOWTRAN-3B model atmosphere, N_b is calculated from Eq. (10), the receiver telescope collecting area is 0.611 m^2, and the total measurement period is 15 minutes. The remaining parameters are summarized in Table II.

In addition, the lower part of Table II shows, for each PMT, the calculated maximum background count rates (N_b) for both day and moonlit night, and the

Table II. Additional Parameters for Lidar Performance Calculations, Plus Lidar Maximum Signal Levels

Wavelength (nm)	355			532		
Laser output (J/pulse)	0.22			0.40		
Transm. opt. eff.	0.96			0.96		
Filter FWHH (nm)	5.0			2.5		
PMT number	1	2	3	4	5	6
Rec. & PMT opt. eff.	2.46E-4	.00279	.0614	1.25E-4	.00380	.119
Range resol. (Δr, km)	.60	1.20	2.40	.60	1.20	2.40
Time resol. (μsec)	4	8	16	4	8	16
Meas. period (minutes)	5	10	15	5	10	15
Total time/Δr (msec)	12.0	48.0	144.1	12.0	48.0	144.1
Altitude Z_s (km)	20	34	52	20	34	52
N_s(max) at Z_s (cts/μsec)	2.37	.88	.69	2.66	2.35	2.47
Night(moon) N_b (cts/μsec)	8.4E-7	9.6E-6	2.1E-4	4.0E -7	1.2E-5	3.8E-4
Day N_b (cts/μsec)	.84	9.6	211.	.47	14.2	444.

lidar backscatter signal maximum count rates (N_S) for each PMT. These N_S values are the maximum for each PMT as obtained when it is switched in by its multiplexer (at altitude Z_S). The PMT dark count rates are all 2×10^{-5} per microsecond or less.

As seen from Figure 4, the night time random errors (RE) are all less than 3.5% to altitudes of over 80 km, with the green signal RE not reaching 10% until 96 km altitude. At the highest altitudes, the haze level is usually negligible, allowing the atmospheric density above 80 km to be obtained from the green N_S only. The PMT switching altitudes of 34 and 52 km (see Table II) are based on limiting the maximum total count rates to about 2.5 per microsecond. Given the scaler regular count rate capability of 100 mHz and the fast PMTs and discriminator circuits to be used, such a random count rate will register about 2.5% too low due to coincidences. A correction[4] for this source of error is easily calculated, and will actually allow meaningful count measurements for corrected rates exceeding 10 per microsecond. The lower limit is used to keep the correction small.

As indicated by Figure 4, reduced accuracy daytime measurements can be made to altitudes of 35-45 km. The day background count rates N_S shown in Table II indicate daytime rates which limit good measurements to PMTs 1 and 4, with only marginal measurements by PMTs 2 and 5. High altitude PMTs 3 and 6 will be overdriven by the day sky background, and must be blocked during daytime use. The lidar system could be optimized for somewhat better daytime performance but only at the loss of some nighttime performance which was given higher priority.

5. REFERENCES

1. M.C.W.Sandford, J. Atmos. Terr. Phys. 29, 1657 (1967).
2. P.McCormick, E.Silverberg, S.Poultney, U.VanWigh, C.Alley, and R.Bettinger, Nature 215, 1262 (1967).
3. M.L.Chanin and A.Hauchecorne, "Lidar Observations of Density Waves and Temperatures in the Stratosphere and Mesosphere," presented at Tenth International Laser Radar Conference, Silver Spring, MD (October 6-9, 1980).
4. G.S.Kent, P.Sandland, and R.Wright, J. Appl. Meteor. 10, 443 (1971).

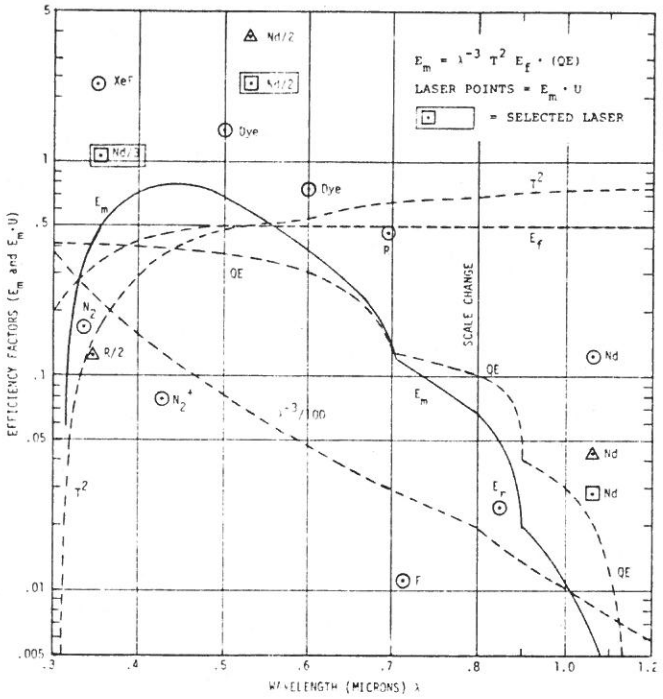

Figure 1. Lidar and Laser Wavelength Trade-off

Lidar efficiency E_m (solid line), its components (dashed lines), and lidar efficiency times maximum useful output ($E_m \cdot U$ points) are all plotted against wavelength. Laser points are generally shown as circles, except triangles are used for frequency-doubled lasers and squares are used for frequency-tripled lasers.

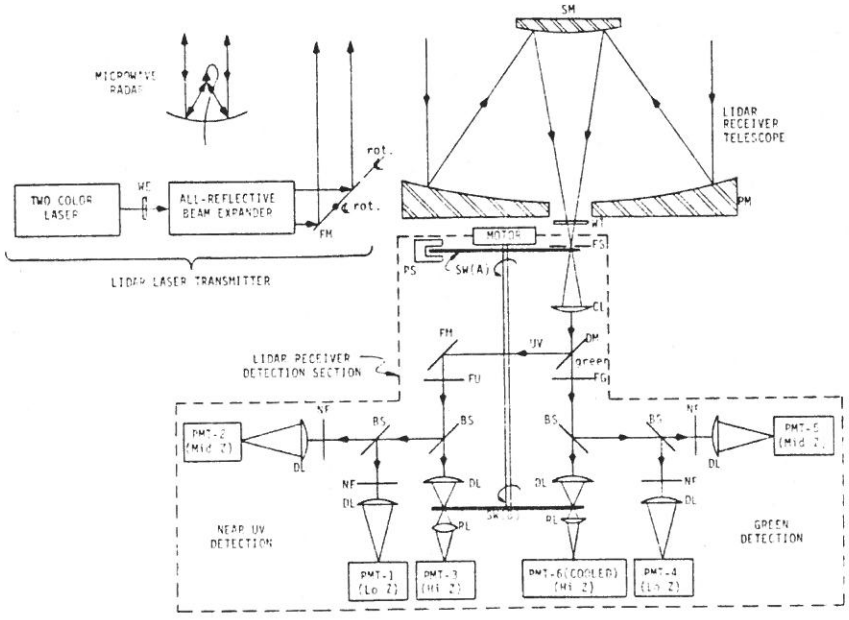

Figure 2. Simplified Optical Block Diagram

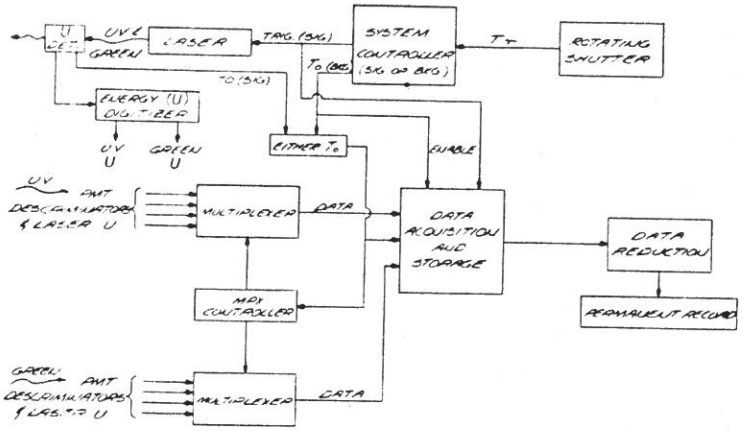

Figure 3. Simplified Electronic Block Diagram

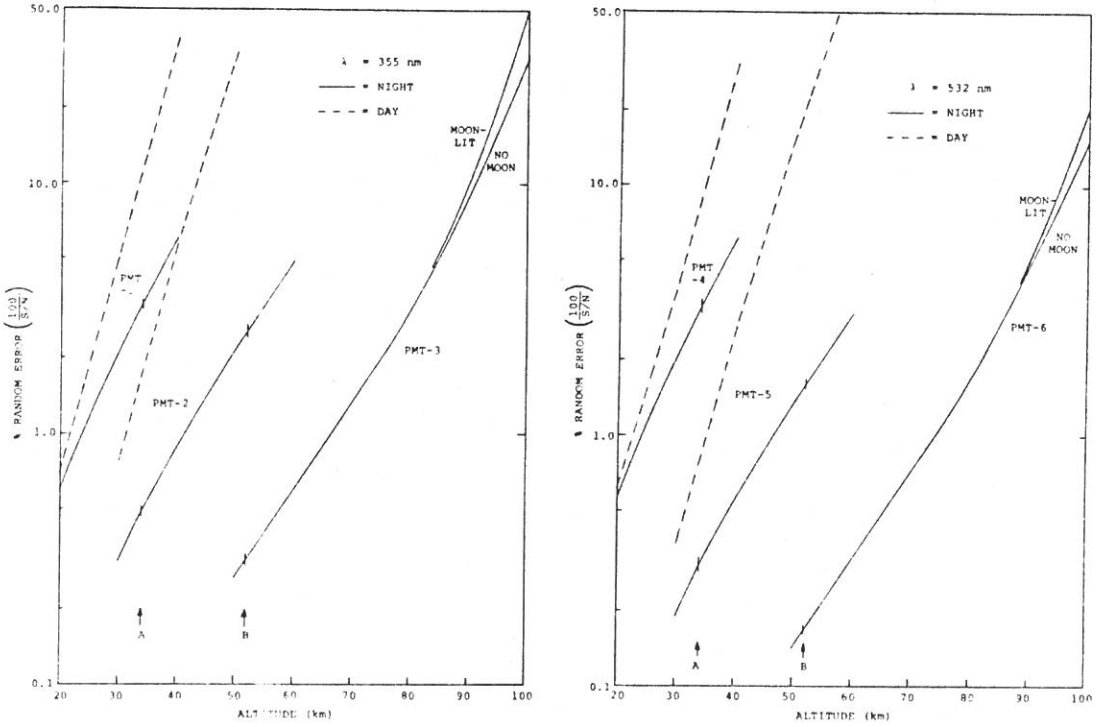

Figure 4a

Figure 4b

Figure 4. Lidar Random Error vs Altitude

Percent random error of the UV (a) and green (b) backscattered lidar signal is shown for a clear night sky background (solid lines) and for a clear day sky background (dashed lines).